Article

Cell Reports

Intrinsically Disordered Regions Can Contribute Promiscuous Interactions to RNP Granule Assembly

Graphical Abstract

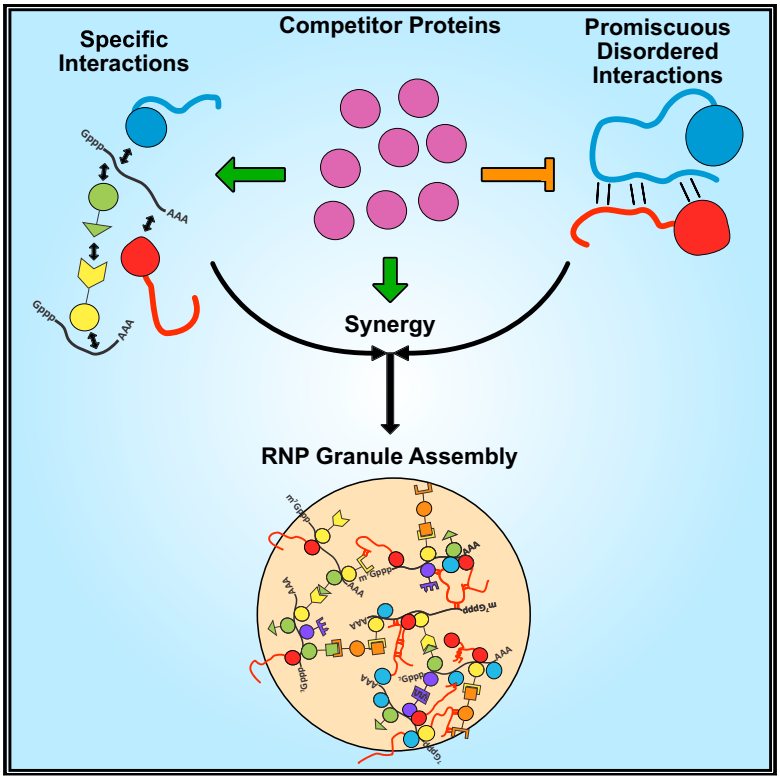

Highlights

- IDRs of proteins interact promiscuously with other proteins
- IDRs can synergize with folded domains to promote phase separation
- Synergy between IDRs and folded domains can lead to RNP granule assembly

Authors

David S.W. Protter, Bhalchandra S. Rao, Briana Van Treeck, Yuan Lin, Laura Mizoue, Michael K. Rosen, Roy Parker

Correspondence

roy.parker@colorado.edu

In Brief

Many RNA-binding proteins contain disordered regions. Protter et al. find that these regions interact nonspecifically with other proteins, which can disrupt phase separation *in vitro*. They also find that promiscuous interactions synergize with specific interactions to promote phase separation and formation of higher-order structures, like RNP granules.

Protter et al., 2018, Cell Reports *22*, 1401–1412
February 6, 2018
https://doi.org/10.1016/j.celrep.2018.01.036

CellPress

Cell Reports
Article

Intrinsically Disordered Regions Can Contribute Promiscuous Interactions to RNP Granule Assembly

David S.W. Protter,[1] Bhalchandra S. Rao,[1] Briana Van Treeck,[1] Yuan Lin,[2] Laura Mizoue,[1] Michael K. Rosen,[2] and Roy Parker[1,3,*]
[1]Department of Chemistry and Biochemistry, Howard Hughes Medical Institute, University of Colorado, Boulder, CO 80309, USA
[2]Department of Biophysics, Howard Hughes Medical Institute, University of Texas Southwestern Medical Center, Dallas, TX 75390, USA
[3]Lead Contact
*Correspondence: roy.parker@colorado.edu
https://doi.org/10.1016/j.celrep.2018.01.036

SUMMARY

Eukaryotic cells contain large RNA-protein assemblies referred to as RNP granules, whose assembly is promoted by both traditional protein interactions and intrinsically disordered protein domains. Using RNP granules as an example, we provide evidence for an assembly mechanism of large cellular structures wherein specific protein-protein or protein-RNA interactions act together with promiscuous interactions of intrinsically disordered regions (IDRs). This synergistic assembly mechanism illuminates RNP granule assembly and explains why many components of RNP granules, and other large dynamic assemblies, contain IDRs linked to specific protein-protein or protein-RNA interaction modules. We suggest assemblies based on combinations of specific interactions and promiscuous IDRs are common features of eukaryotic cells.

INTRODUCTION

Eukaryotic cells contain several non-membrane bound RNA-protein assemblies, referred to as RNP granules. Such RNP granules include the nucleolus and Cajal bodies in the nucleus, as well as stress granules and P-bodies in the cytosol (Spector, 2006). RNP granules are dynamic, as judged by FRAP of their protein components, and exhibit liquid-like behaviors, such as flowing, fusing, and rapid reorganization of internal components (Brangwynne, 2013; Brangwynne et al., 2009). RNP granules are thought to assemble through a process referred to as liquid-liquid phase separation (LLPS), wherein RNA molecules provide binding sites for RNA-binding proteins that interact with themselves or other RNA-binding proteins to create a larger multivalent assembly (Elbaum-Garfinkle et al., 2015; Feric et al., 2016; Mitrea et al., 2016; Nott et al., 2015; Pak et al., 2016; Patel et al., 2015; Zhang et al., 2015). Some of the interactions that drive RNP granule assembly are well defined interactions between folded proteins, or folded protein domains and short linear motifs (SLiMs) (Jonas and Izaurralde, 2013; Kedersha et al., 2016; Mitrea et al., 2016). Because these interactions require folded protein structures and/or extended linear motifs that interact in a stereospecific manner, we refer to these interactions as specific interactions.

The IDRs of RNA-binding proteins have been highlighted as drivers of RNP granule assembly for three reasons. First, genetics indicate that IDRs can be important for assembly of RNP granules or localization of granule components (Decker et al., 2007; Feric et al., 2016; Gilks et al., 2004; Hennig et al., 2015). Second, RNP granules are often enriched in proteins with IDRs (Decker et al., 2007; Jain et al., 2016; Kato et al., 2012; Reijns et al., 2008). Finally, IDRs are often (but not always) both necessary and/or sufficient for LLPS of granule proteins *in vitro*, forming structures that resemble RNP granules *in vivo* (Elbaum-Garfinkle et al., 2015; Lin et al., 2015; Molliex et al., 2015; Nott et al., 2015; Patel et al., 2015; Smith et al., 2016; Zhang et al., 2015).

An unresolved issue is how IDRs contribute to RNP granule assembly and how IDR-based assembly mechanisms integrate with specific protein-protein and protein-RNA interactions to promote RNP granule formation. The literature suggests three non-mutually exclusive models by which IDRs could contribute to LLPS *in vitro* and RNP granule formation *in vivo*. First, some experiments *in vitro* suggest that IDRs promote LLPS via weak binding, utilizing electrostatic, cation-π, dipole-dipole, and π-π stacking interactions (Brangwynne et al., 2015; Lin et al., 2016; Nott et al., 2015; Pak et al., 2016). Charge patterning also appears to play an important role, wherein like-charged amino acids are clustered together within an IDR. Scrambling these charges across the length of an IDR has been observed to impair LLPS both *in vitro* and *in vivo* (Nott et al., 2015; Pak et al., 2016). Because these interactions only require a few amino acids, and do not require any stereospecific arrangement, they would be anticipated to occur between an IDR and many other proteins, including other IDRs. Indeed, charge patterning specifically has been proposed to mediate interactions between IDRs and cellular proteins (Pak et al., 2016). For this reason, we refer to the above types of IDR interactions as nonspecific. These interactions will also be promiscuous, because they will be relatively indiscriminate with respect to binding partners. A second possibility is that elements within some IDRs interact in a specific manner involving local regions of secondary structure. For

example, a locally formed α-helix in TDP-43 can mediate LLPS through homotypic interactions (Conicella et al., 2016), and relatively short regions containing aromatic residues in disordered regions can form self-interaction motifs referred to as LARKS (Hughes et al., 2017). Finally, it is likely that a subset of IDRs are also promiscuous RNA-binding proteins since they can be rich in positive charges, some IDRs can cross link to mRNA *in vivo*, and some IDRs can bind RNA *in vitro* (Lin et al., 2015; Molliex et al., 2015).

Given the promiscuous nature of at least some IDR interactions, we hypothesized that such IDR-based interactions alone would be susceptible to other highly abundant proteins in cells and therefore insufficient to drive LLPS and the assembly of RNP granules *in vivo*. In the context of the protein-rich cellular environment, other proteins would compete for binding to the IDRs and thereby prevent their forming a defined assembly. Moreover, even the ability of some IDRs to form specific local interacting structures might be impaired by competition with other proteins in the cell. Instead, to account for the contributions from both IDRs and specific interactions to RNP granule assembly, we hypothesized that IDRs would reinforce assemblies that contained specific assembly interactions. Effectively, specific interactions would concentrate the IDRs and strengthen their interactions through additive binding energies (Jencks, 1981), either biasing their promiscuous interactions toward components of the assembly, or promoting the formation of specific, albeit weaker, interactions between the IDRs such as LARKS (Hughes et al., 2017). In this way, IDR-based interactions could contribute to the energetics of assembly.

Here, we provide several observations that RNP granule assembly gains selectivity from specific protein-protein and protein-RNA interactions, and promiscuous binding of IDRs to proteins and possibly RNA enhances these assemblies. First, we observe that LLPS driven by IDRs *in vitro* is inhibited by other proteins. Second, in cells, we observe that IDRs of granule components are often neither required nor sufficient to target proteins to RNP granules. Third, we demonstrate that *in vitro* LLPS driven by specific protein-RNA interactions is enhanced by adding promiscuously interacting IDRs, and the assembly of yeast P-bodies in cells is promoted by nonspecific IDRs in conjunction with specific interactions. Thus, RNP granules assemble primarily by specific interactions, which can be enhanced by IDRs capable of either promiscuous, or weak specific interactions based on small structural elements that become effective at high local concentrations. We suggest that this general assembly mechanism may be shared by other macromolecular complexes rich in IDRs.

RESULTS

Several Proteins Inhibit LLPS Driven by IDRs *In Vitro*

We hypothesized that IDRs of RNA-binding proteins might not be sufficient to drive LLPS in the presence of other proteins similar to the intracellular environment, despite the observation that such IDRs are capable of undergoing LLPS as purified proteins (Elbaum-Garfinkle et al., 2015; Lin et al., 2015; Molliex et al., 2015; Nott et al., 2015; Patel et al., 2015; Smith et al., 2016; Zhang et al., 2015). Our hypothesis was based on the observations that LLPS driven by IDRs *in vitro* are thought to occur by weak electrostatic, dipolar interactions as well as interactions involving aromatic groups (Brangwynne et al., 2015). Because these interactions are nonspecific, they are likely relatively promiscuous and could, in principle, occur between an IDR and other IDRs or with many other proteins. Moreover, even IDRs that have homotypic interactions based on local structural elements might be sensitive to other proteins and be most efficient at forming such specific assemblies only in conjunction with specific interactions (Conicella et al., 2016; Xiang et al., 2015). Thus, we asked whether IDR-driven LLPS *in vitro* would be inhibited in the presence of other polypeptides, which would be analogous to the interior of the cell.

To test whether an IDR can promote LLPS in the presence of other proteins, we induced LLPS of either full-length hnRNPA1$_{\Delta hexa}$ or only the hnRNPA1$_{IDR}$ region (amino acids 186–320, Figure 1A) by dilution into lower salt (37 mM NaCl) (Lin et al., 2015) in the presence of increasing amounts of BSA. We used the Δhexa-peptide variant of the full-length hnRNPA1 protein as it is less prone to forming amyloid fibers during purification and analysis and behaves similarly to the wild-type protein with regards to LLPS (Kim et al., 2013; Lin et al., 2015; Molliex et al., 2015). Unless otherwise noted, the fluorescently conjugatable SNAP tag was fused with all purified proteins in order to visualize droplets.

As the concentration of BSA increased, LLPS for both full-length SNAP-hnRNPA1$_{\Delta hexa}$ and the SNAP-hnRNPA1$_{IDR}$ was inhibited (Figure 1B). At higher BSA concentrations, we observed the formation of some aggregated SNAP-hnRNPA1$_{\Delta hexa}$ and SNAP-hnRNPA1$_{IDR}$ that contrast with the liquid droplets seen in the absence of BSA (Figure 1B). As BSA concentrations increase, droplet sizes decrease and no large droplets form (Figure 1C). Interestingly, by looking at a subset of droplets of similar size across all BSA concentrations, we noticed that as BSA concentrations increased the intensities of SNAP-hnRNPA1$_{\Delta hexa}$ droplets decreased (Figure 1D). The distribution of droplet areas was approximately equal between samples (Figure 1D, inset). As mentioned above, an amorphous precipitate forms at higher BSA concentrations, as assemblies get dimmer. While this precipitate may represent a third phase, contributing to some of the loss of fluorescence intensity, the overall area is much smaller than the droplets (Figures 1C and 1D). Because both the area and intensity of aggregates are less than the droplets, this suggests that much of the protein within droplets moves to the soluble phase at higher BSA concentrations. The partition coefficient of LLPS (the ratio of protein within the concentrated phase versus within the dilute phase) is a measure of the equilibrium between the two states. Therefore, we interpret this decrease in intensity to mean that BSA shifts the phase separation equilibrium to one less favorable for SNAP-hnRNP A1$_{\Delta hexa}$ to exist within the concentrated phase. At higher BSA concentrations the equilibrium shifts such that SNAP-hnRNPA1$_{\Delta hexa}$ is below the critical concentration for LLPS. Thus, BSA is an inhibitor of LLPS driven by SNAP-hnRNPA1 or its IDR alone under these conditions.

To determine if this inhibitory effect is unique to hnRNPA1 and BSA, we examined how untagged BSA, lysozyme, and RNase A affected LLPS driven by IDRs found in hnRNPA1, FUS, or eIF4GII,

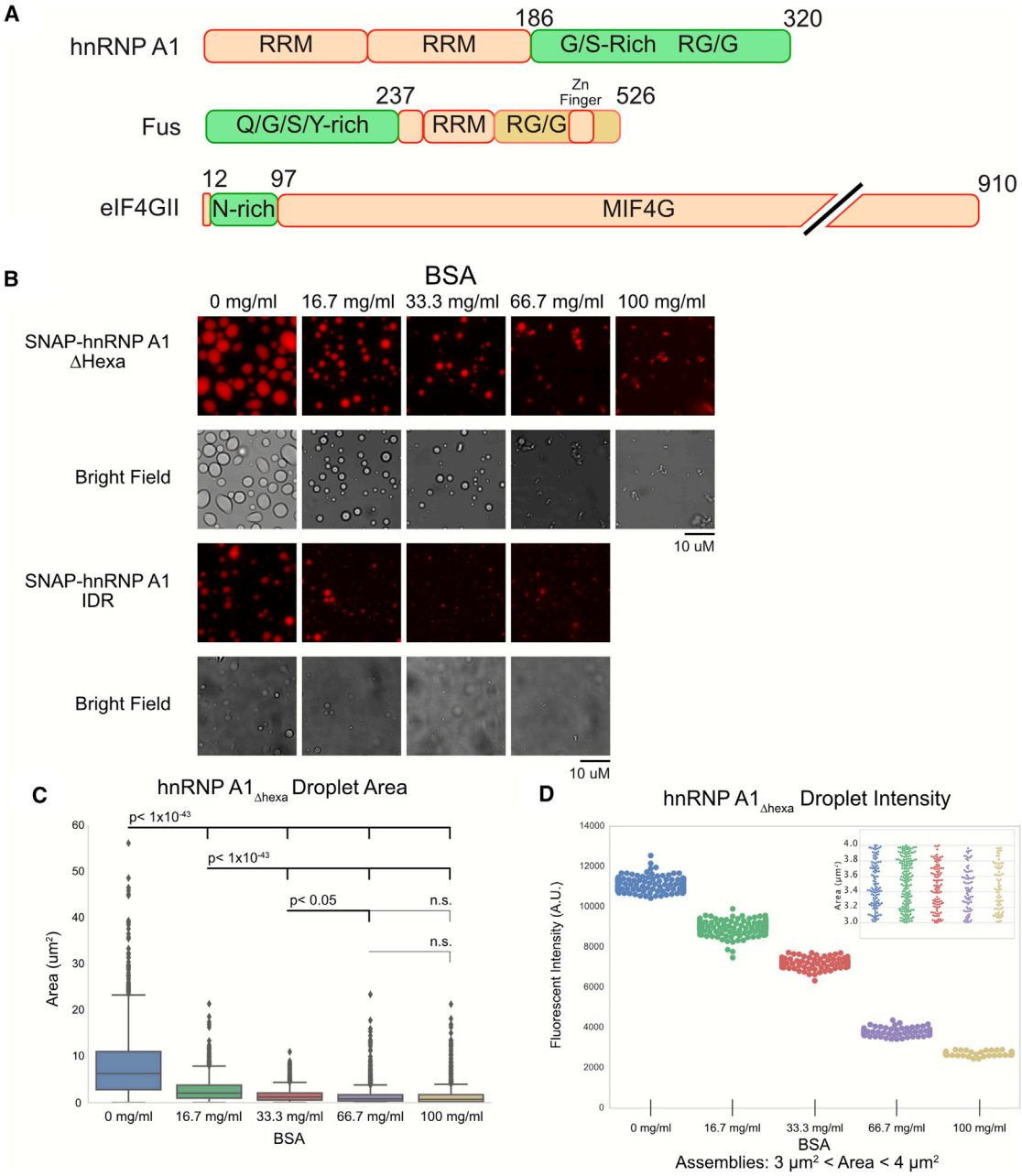

Figure 1. Competitor Proteins Disrupt IDR-Driven Phase Separations

(A) Domain structure of hnRNP A1, FUS, and eIF4GII.

(B) Fluorescent and bright-field microscopy images of phase separated droplets formed at 37.5 mM NaCl by 25 μM SNAP-hnRNP $A1_{IDR}$ or 2.1 μM SNAP-hnRNP $A1_{IDR}$ with the indicated concentrations of BSA. Images each independently scaled.

(C) Box and whisker plot of structure size for SNAP-hnRNP A1Δhexa from (B), significance calculated with Welch's t test for unequal size and variance. Whiskers indicate distribution limits, excluding outliers.

(D) Quantification of the intensity of all structures between areas of 3 μm and 4 μm for hnRNP $A1_{\Delta hexa}$ from (B). Subsets of droplets have roughly equal distributions of size (inset).

which have been reported to undergo LLPS at low salt or low temperature (Lin et al., 2015; Molliex et al., 2015). We observed that LLPS of SNAP-FUS_{IDR} (FUS amino acids 1–237), SNAP-$eIF4GII_{IDR}$ (eIF4GII amino acids 13–97), or SNAP-$hnRNPA1_{IDR}$ (Figure 1A) were also inhibited by the presence of BSA, lysozyme, or RNase A (Figure 2A).

To more closely mimic the cellular environment, we examined whether IDRs or IDR containing proteins could undergo LLPS

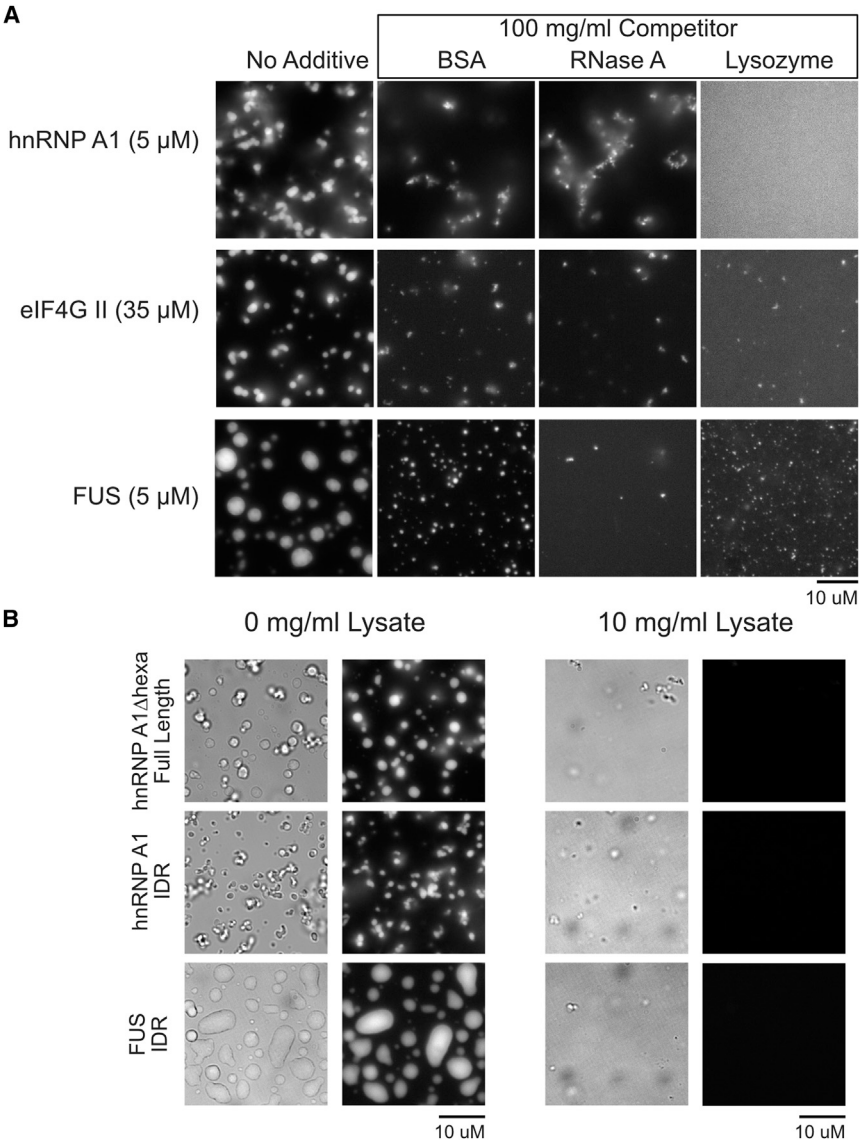

Figure 2. Disruption of LLPS by Other Proteins Is a General Phenomenon

(A) Phase-separated droplets formed at 37.5 mM NaCl by SNAP-hnRNP $A1_{IDR}$, SNAP-FUS_{IDR}, SNAP-$eIF4GII_{IDR}$ in the absence or presence of 100 mg/mL BSA, lysozyme, or RNase A. Images each independently scaled.

(B) Phase-separated droplets formed at 37.5 mM NaCl by SNAP-hnRNP $A1_{\Delta hexa}$, SNAP-hnRNP $A1_{IDR}$, and SNAP-FUS_{IDR} in the absence or presence of ~10 mg/mL yeast lysate. Pairs of fluorescent images are scaled to the 0 mg/mL image.

in the presence of yeast lysate, which had been previously depleted of small metabolites and exchanged into droplet-forming buffer via desalting columns. We observed that LLPS of SNAP fusions of hnRNPA$1_{\Delta hexa}$, hnRNPA1_{IDR}, and FUS_{IDR} are all strongly impaired in yeast lysates, which contained ~10 mg/mL protein (Figure 2B). Yeast lysates are our closest approximation of the cellular environment, and we find that even lysates ~1/10th as concentrated as the cell (Milo, 2013) strongly impair LLPS of IDRs. Thus, phase separation of multiple IDRs is sensitive to competition from other molecules within the cell.

Competitor Proteins Inhibit LLPS *In Vitro* by Interacting with IDRs

What is the mechanism by which competitor proteins inhibit IDR-driven LLPS *in vitro*? One possibility is that BSA, lysozyme, and RNase A share some specific property or structural feature that inhibits LLPS of these IDRs. This is unlikely as BSA, lysozyme, and RNase A are structurally unrelated, and vary in size (66.4, 14.3, and 13.7 kDa, respectively) and pI (5.3, 11.35, and 9.6, respectively). A second possibility is that any crowding agent will inhibit LLPS under these conditions. However, we observe that LLPS driven by hnRNPA1_{IDR} is stimulated by the crowding agents Ficoll and PEG, with phase separation occurring at higher ionic strengths and lower protein concentrations than without crowding agents (Figure S1A) (Lin et al., 2015; Molliex et al., 2015).

A third possibility is that these competitor proteins compete for promiscuous interactions between IDRs and thereby disrupt LLPS. A prediction of this model is that at low concentrations, insufficient to block LLPS, the competitor proteins would be recruited into the phase separated droplets (due to interactions with the IDR). To test this possibility, we examined the recruitment of directly labeled fluorescent BSA or lysozyme into droplets formed by IDRs. At low concentrations both proteins were recruited to IDR-driven droplets without disrupting the assemblies. For example, at 500 nM concentration fluorescein isothiocyanate (FITC)-BSA was strongly enriched in droplets of SNAP-hnRNPA$1_{\Delta hexa}$ (Figure 3A). FITC-lysozyme was also recruited (Figure 3A). Similarly, droplets of SNAP-$eIF4GII_{IDR}$, SNAP-hnRNPA1_{IDR}, and SNAP-FUS_{IDR} all recruited both FITC-BSA and FITC-lysozyme (Figure 3B). Importantly, neither FITC-PEG nor FITC-Ficoll were enriched in droplets of SNAP-hnRNP $A1_{\Delta hexa}$ (Figures S1B and S1C). This suggests that these IDRs can interact with both BSA and lysozyme, consistent with the idea that competitor proteins could compete with the weak interactions that mediate LLPS.

The recruitment of other macromolecules to these assemblies suggests that these *in vitro* protein droplets may be complex coacervates. Complex coacervates are phase-separated systems containing multiple kinds of macromolecules, typically expected to interact through opposing charges (Pak et al., 2016). This also

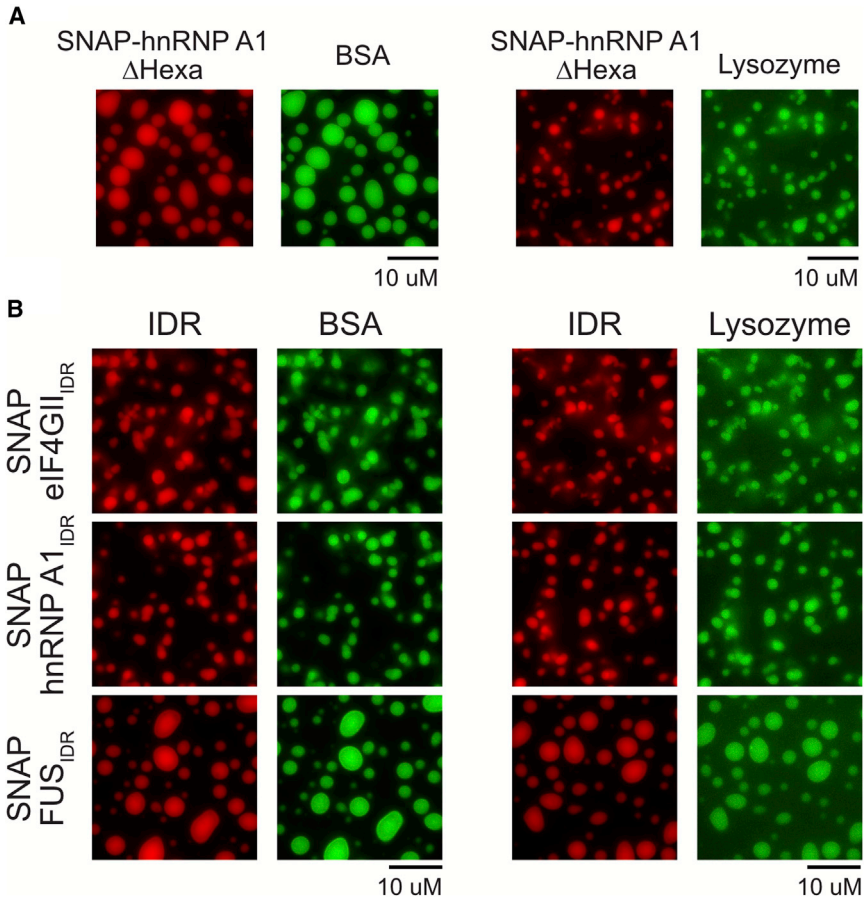

Figure 3. Globular Proteins Are Recruited to IDR-Driven LLPS Droplets

(A) Phase-separated droplets formed at 37.5 mM NaCl by 25 μM SNAP-hnRNP A1$_{\Delta hexa}$ and 500 nM FITC-labeled BSA or FITC-labeled lysozyme. Images each independently scaled.

(B) Phase-separated droplets formed by SNAP-eIF4GII$_{IDR}$ (35 μM), SNAP-hnRNP A1$_{IDR}$ (5.25 μM), or SNAP-FUS$_{IDR}$ (5 μM) in the presence of either 10 nM FITC-BSA or 100 nM FITC-lysozyme. Images each independently scaled.

suggests that other protein components in our mixtures, such as TEV or MBP, may in fact be found in and contribute to the droplet phase. While we have not investigated this possibility here, it is important to consider the possibility of complex coacervation in these *in vitro* systems. In theory, in some systems complex coacervation could lead to an increased propensity for phase separation. Indeed, we see that some concentrations of lysozyme (8.33 mg/mL and 16.66 mg/mL) have the ability to stimulate SNAP-FUS$_{IDR}$ droplet formation (Figure S1D). As the concentration of lysozyme increases, it then begins to inhibit assembly. This stimulatory behavior was not observed for either BSA or RNase A (Figure S1D). While complex coacervation can stimulate assembly, at higher concentrations of competitor proteins, inhibition of assembly was always observed (Figures 1, 2, and S1D).

The above evidence suggests that competitor proteins can interact with IDRs, both because these proteins are recruited into phase-separated droplets and because they inhibit LLPS at higher concentrations. Because these proteins were chosen at random and have diverse physical properties, and LLPS is also inhibited by metabolite-depleted cell lysates, we suggest that IDRs by themselves are likely to be susceptible to such nonspecific interactions in the more complex cellular environment. Therefore, in many cases, promiscuous interactions of IDRs are unlikely to be sufficient for RNP granule assembly in cells.

IDRs Can Enhance LLPS Driven by Specific Interactions in the Presence of Competitor Proteins

The *in vitro* results above suggest that IDR-IDR interactions are susceptible to competition by the complex protein mixture in the cell. However, IDRs are enriched in RNP granule proteins (Decker et al., 2007; Jain et al., 2016; Kato et al., 2012; Reijns et al., 2008), and IDRs can play a role in RNP granule assembly (Decker et al., 2007; Gilks et al., 2004). In some cases, IDRs contain SLiMs that are important for assembly of RNP granules (Jonas and Izaurralde, 2013). However, because there are cases wherein one IDR can functionally substitute for another in RNP granule assembly (Decker et al., 2007; Gilks et al., 2004), a more generic role for IDRs in RNP granule assembly is also likely.

We hypothesized that IDRs in proteins that also make specific interactions could provide promiscuous, nonspecific interactions that stabilize an RNP granule by acting together with the specific interactions. By concentrating the IDRs through specific interactions, promiscuous IDR-based interactions are biased to other components of the assembly. In this model, specific interactions and nonspecific interactions both donate binding energy that promotes LLPS. This model makes two predictions that we first tested *in vitro*.

First, the model predicts that LLPSs driven by specific interactions should be less susceptible to the interference from other competitor proteins, and may even be enhanced, given that high concentrations of such proteins can serve as crowding agents. Consistent with this view, we have shown that the LLPS driven by the specific interaction of an RNA-binding protein, poly-pyrimidine tract binding protein (PTB), with RNA is promoted by BSA (Li et al., 2012; Lin et al., 2015), reproduced here. For example, while SNAP-tagged PTB and RNA showed limited assembly when mixed together at concentrations of 20 μM and 1.6 μM, respectively, the addition of 100 mg/mL BSA induced robust phase separation at these concentrations (Figure 4A). Consistent with this effect being due to molecular crowding, PTB-RNA LLPS is also stimulated by PEG or Ficoll, additional crowding agents (Figure 4A). However, it is also possible that BSA is contributing via formation of a complex coacervate. In

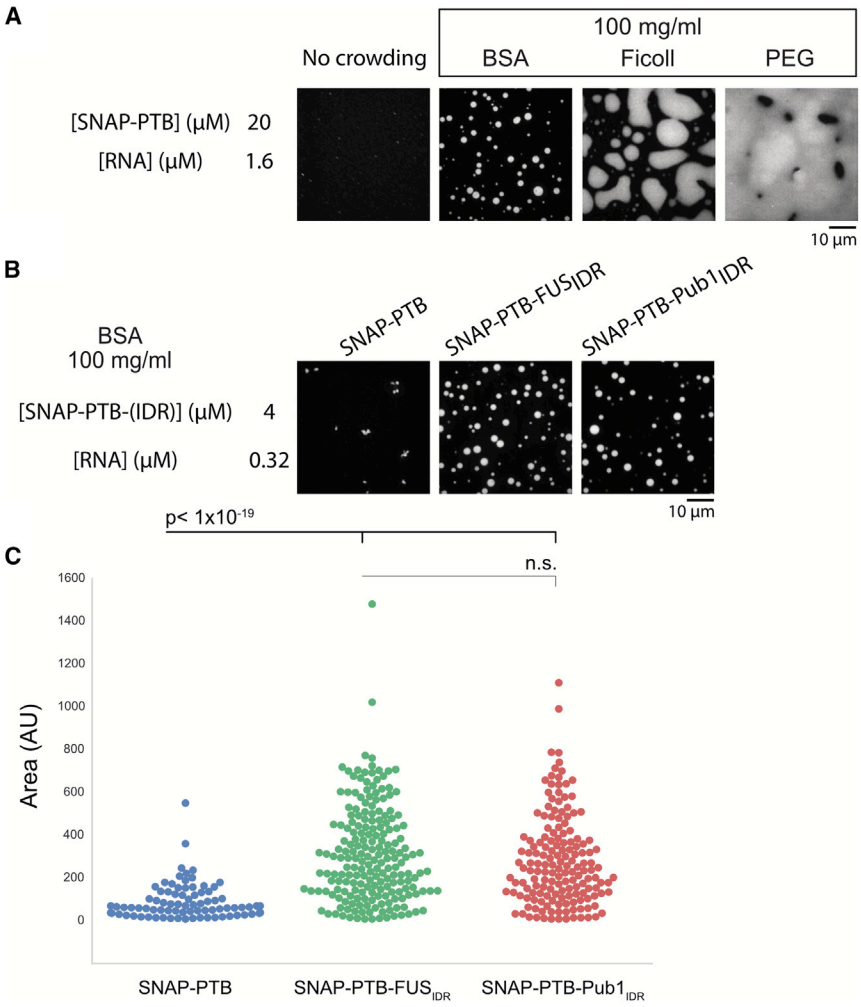

Figure 4. IDRs Enhance LLPS of PTB plus RNA in the Presence of BSA

(A) Phase-separated droplets formed by SNAP-PTB and RNA in the presence or absence of 100 mg/mL BSA, Ficoll, or PEG.

(B) Phase-separated droplets of 4μM SNAP-PTB, SNAP-PTB-FUS_{IDR}, or SNAP-PTB-$Pub1_{IDR}$, plus 0.32 μM RNA assemblies in the presence or absence of 100 mg/mL BSA.

(C) Quantification of assembly area for (B) with arbitrary units. Welch's t test.

either case, the specific PTB-RNA interactions are not outcompeted by BSA, allowing for phase separation to occur even in the presence of competitor protein.

A second prediction of the model is that although IDRs alone are not sufficient to drive phase separation in the presence of competitor proteins, IDRs would contribute binding energy to phase separation driven by specific interactions, decreasing the threshold concentration of assembly. To test this prediction, we examined how IDRs affect PTB-RNA phase separation in the presence of competitor proteins. For example, 4 μM PTB and 0.32 μM RNA do not phase separate in 100 mg/mL BSA. However, we observed LLPS with identical concentrations of RNA and SNAP-PTB, when SNAP-PTB was fused to either the FUS or Pub1 IDRs (Figure 4B). SNAP-PTB fused to either IDR showed an increase in both the number and size of the assemblies visualized (Figure 4C). We have previously observed that under similar conditions neither of these IDRs phase separates with RNA (Lin et al., 2015), suggesting this is not the driving factor for enhancement of LLPS. Therefore, weak interactions of IDRs can enhance phase separation in the presence of competitor proteins, when present in molecules that also contain specific interactions which are less susceptible to competition from cellular macromolecules.

IDRs Are Often Neither Sufficient nor Necessary *In Vivo* to Target Components to RNP Granules

An assembly mechanism for RNP granules driven by specific interactions aided by promiscuous interactions of IDRs has predictions for how components would be recruited to RNP granules. Specifically, one would predict that generally IDRs would not be sufficient to target a protein to an RNP granule, unless they contained a specific SLiM. Moreover, IDRs would not be required for recruitment to a granule, although they could affect the partition coefficient (the concentration of a component within versus outside of a granule).

To examine how IDRs of yeast proteins affect their targeting to P-bodies, we examined if IDRs within Lsm4, Dhh1, Pop2, and Ccr4 (Figure 5A) were necessary and/or sufficient for their recruitment into P-bodies. The IDRs of Lsm4, Dhh1, Pop2, and Ccr4 were fused separately to either GFP or mCherry (Table S1). IDR-fusion proteins were expressed in yeast co-expressing a chromosomally GFP-tagged P-body component or containing a secondary plasmid containing a mCherry tagged P-body component. These strains still expressed the endogenous versions of these fusion proteins. P-bodies were induced by glucose deprivation for 15 min, and the percentage of P-bodies containing the IDR fusion protein was counted. For example, clear enrichment in P-bodies was detectable for full-length Dhh1 (Figure 5B). However, the Dhh1 IDR was not sufficient for P-body localization (Figure 5B). Similarly, the IDRs of Lsm4, Pop2, and Ccr4, were insufficient for recruitment of GFP to P-bodies (Figure 5C). We then removed these IDRs from their full-length proteins and found that deletion of the IDRs in Dhh1, Lsm4, Ccr4 had little to no effect on their recruitment to P-bodies (Figures 5B and 5C). However, for the already poorly localized Pop2, deletion of the IDR did have a noticeable impact on localization (Figure 5C). Thus, the IDRs of Dhh1, Lsm4, Ccr4, and Pop2 are not sufficient for GFP recruitment into P-bodies but

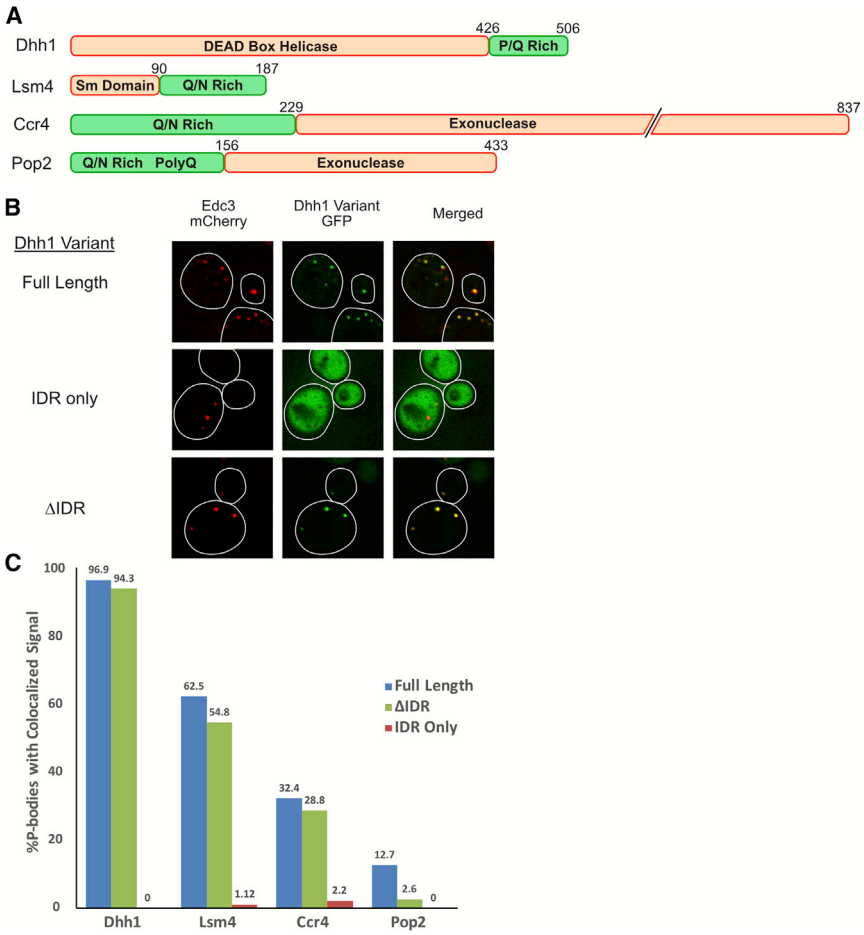

Figure 5. IDRs Are Neither Sufficient nor Required for P-Body Localization

(A) Domain structures of the yeast proteins Dhh1, Lsm4, Ccr4, and Pop2.

(B) Dhh1-GFP variant fusions were expressed in Edc3-mCherry expressing yeast. P-bodies were visualized by fluorescence microscopy after 10 min glucose deprivation.

(C) Quantification of the percentage of P-bodies that exhibited colocalization with the expressed fusion protein. GFP was fused to the N terminus of Dhh1, Ccr4, and Pop2 variants. Variants were co-transformed with Edc3-mCherry. mCherry was fused to the C terminus of the Lsm4 variants, which were expressed in cells with genomically tagged Dcp2-GFP (>100 foci counted per condition). See Table S1.

may contribute to protein localization in cases where recruitment is already poor such as Pop2.

IDRs Can Enhance LLPS Driven by Specific Interactions in Cells

The observations above suggest cellular assemblies such as RNP granules may form with assembly primarily driven by a set of specific interactions, with the prevalence of IDR regions in such assemblies contributing either a second set of promiscuous nonspecific interactions that would enhance assembly, or having specific interactions with themselves that require high local concentrations to form. Some IDRs do contribute to RNP granule assembly in genetic backgrounds that limit assembly. For example, the C-terminal IDR of Lsm4 is not required for P-body assembly normally, but plays a role in a strain lacking the P-body scaffold protein Edc3 (Decker et al., 2007).

To determine if this may be a more general phenomenon, we examined how the C-terminal IDR of the yeast Dhh1 protein promotes P-body formation. In *edc3*Δ *lsm4*Δ*C* yeast strains, which lack visible P bodies, P-body formation can be partially rescued by the addition of a single copy plasmid providing an extra copy of the Dhh1 gene, which through specific interactions with RNA and Pat1 enhances P-body assembly (Rao and Parker, 2017). Overexpression of Dhh1 in an *edc3*Δ *lsm4*Δ*C* background creates a cellular context where P-bodies are just above the threshold for assembly. Dhh1 also has a C-terminal P/Q rich IDR (Figure 5). To determine whether this C-terminal IDR contributes to P-body assembly, we compared the ability of full-length Dhh1 and a Dhh1ΔIDR truncation (1–427), which lacks the C-terminal IDR (residues 428–506), to rescue P-body formation in an *edc3*Δ *lsm4*Δ*C* strain.

We found that wild-type Dhh1 rescues P-body formation in the *edc3*Δ *lsm4*Δ*C* strain, yet the Dhh1ΔIDR variant fails to do so (Rao and Parker, 2017) (Figures 6A and 6B), despite being expressed at levels similar to the full-length protein (Figure S2A). This demonstrates that the C-terminal IDR of Dhh1, while not required for P-body formation normally, can contribute additional interactions that enhance the formation of P-bodies when granule assembly is partially impaired.

In principle, the IDR of Dhh1 could provide a specific interaction, perhaps containing a SLiM, or a promiscuous interaction as we observed for several IDRs *in vitro*. If the Dhh1-IDR makes a specific interaction, then it should not be functionally replaceable by other IDRs capable of promiscuous interactions. Alternatively, if this IDR simply provides additional promiscuous interactions then any IDR capable of such interactions should functionally replace the Dhh1-IDR in promoting P-body assembly. To distinguish between these possibilities, we determined whether the IDRs of human Lsm4, a P-body component, as well as the IDRs of two human stress granule components, hnRNPA1, and the N-terminal domain of FUS, could replace the function of the Dhh1 IDR. We also tested the disordered regions of a late-embryogenesis abundant (LEA)-like protein, here referred to as LEA-SC (LEA-Group2-like, from the nematode *Steinernema carpocapsae*, amino acids 1–95). LEA proteins are proposed to provide desiccation protection by interacting promiscuously with proteins in the cell, replacing water during desiccation (Hand et al., 2011). We utilized the IDRs of human proteins because these are very unlikely to contain specific binding partners in yeast.

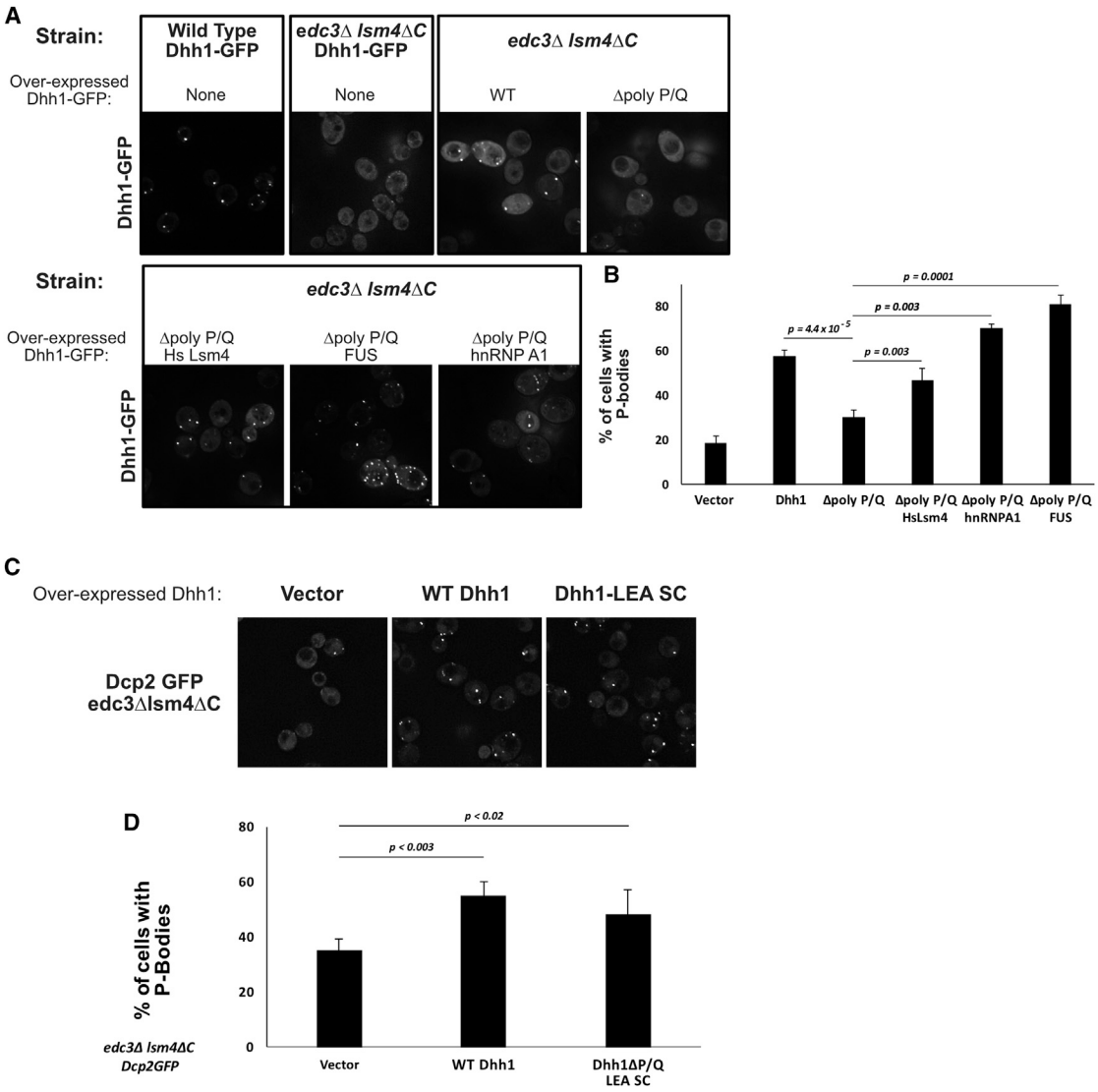

Figure 6. Specific Interactions Can Synergize with Promiscuous Nonspecific Interactions to Drive Assembly

(A) Cells expressing Dhh1-GFP, either genomically or as a plasmid-expressed Dhh1-GFP variant. Cells were deprived of glucose for 10 min to induced P-body assembly.

(B) Quantification of (A), depicting the percentage of cells containing at least one P-body. Error bars, ±SD.

(C) Cells expressing Dhh1 – LEA-SC or wild-type Dhh1. Cells were deprived of glucose for 10 min to induced P-body assembly, and visualized by genomically GFP-tagged Dcp2.

(D) Quantification of (C), percentage of cells with at least one P-body. *p < 0.05. Error bars, ±SD.

All three granule-component IDRs complemented the P-body assembly defect seen in the Dhh1-ΔIDR construct (Figure 6B). Similarly, the LEA-SC protein, also rescued the assembly defect (Figure 6C). Addition of these IDRs does not cause appreciable assembly of large structures without glucose deprivation (Figure S2B), demonstrating these assemblies are indeed P-bodies and not a different constitutive aggregate.

Interestingly, the IDRs tested here are all predicted to have somewhat similar predicted structural characteristics. Not all IDRs have the same behavior in solution, and these different behaviors can be predicted using the CIDER algorithm (Das et al., 2015). Depending on the charge density, overall charge distribution, and overall positive or negative charge, IDRs can behave in a variety of different ways, such as globules, coils/hairpins, or extended swollen coils. Interestingly, all of our IDRs are suggested to be polyampholytes (not enriched for positive or negative charge) that are expected to behave as either globules or coils in solution (Figure S3A). Given this, we suggest at least the generic class of polyampholytes can contribute to RNP granule assembly in a promiscuous manner, and this property might be shared by other classes of IDRs, which we have not tested to date.

These results argue that the Dhh1 IDR does not provide a specific interaction necessary for P-body assembly, as it can be replaced with IDRs from a variety of organisms. This result also demonstrates that multiple different IDRs can complement the Dhh1ΔIDR, consistent with promiscuous, nonspecific interactions of the IDRs contributing to RNP granule assembly in conjunction with specific interactions.

DISCUSSION

RNP granules are cytoplasmic assemblies composed of specific groups of cellular proteins and RNA molecules (Jain et al., 2016). In principle, a specific assembly could be assembled in three manners: (1) solely a set of specific interactions with a set of limited and well-defined binding partners, (2) through a summation of promiscuous interactions, where additive effects of subtle differences in interaction propensity lead to specific assemblies, or (3) through a combination of specific and promiscuous interactions. This third potential mechanism is supported by genetic analyses of the interactions that drive RNP granule assembly as well as our own findings. Specific interactions can clearly be important for assembly. For example, Edc3 dimerization via its YjeF-N domain is important for P-body assembly in yeast (Decker et al., 2007). G3BP dimerization, as well as interactions with caprin, are important for mammalian stress granule assembly (Kedersha et al., 2016). Some specific interactions can involve SLiMs found in IDRs that specifically interact with well-folded domains of other RNA-binding proteins (reviewed in (Jonas and Izaurralde, 2013). One example of this phenomena is the disruption of Dcp2′s localization to P-bodies in yeast caused by deletion of or interference with specific SLiMs in Dcp2′s C-terminal IDR, which interact with a surface of Edc3 (Fromm et al., 2014; Harigaya et al., 2010). Thus, specific interactions between RNA-binding proteins play important roles in formation of P-bodies and recruitment of molecules into them. However, we have also shown that promiscuous interactions can play a role in assembly.

A key contribution of this work is to provide evidence that at least some IDRs function to promote RNP granule assembly both in cells, and in model biochemical systems, through weak interactions that require being coupled to protein domains with specific interactions. First, examination of the FUS, hnRNPA1, and eIF4GII IDRs reveal that they all interact nonspecifically with generic proteins, and those proteins and yeast lysates disrupt their ability to undergo LLPS in isolation (Figures 1 and 2). However, when tethered to the PTB RNA-binding protein, which phase separates in the presence of RNA, promiscuous IDRs can promote LLPS, even in the presence of competitor proteins (Figure 4). Third, the C-terminal P/Q rich IDR of Dhh1 promotes P-body assembly in yeast, and this domain can be replaced by the IDRs of human Lsm4, hnRNPA1, or FUS, or by specific LEA proteins from brine shrimp or nematodes (Figure 6). The contribution of such IDRs to assembly is likely due to the ability of IDRs to promote LLPS through a variety of weak promiscuous interactions including electrostatic, cation-π, dipole-dipole, and π-π stacking interactions (Brangwynne et al., 2015; Nott et al., 2015), which would be enhanced through effects analogous to avidity by coupled specific interactions of adjacent domains (Jencks, 1981).

Additional evidence exists that LLPS can be driven by combined specific and non-specific interactions. For example, even very high expression levels of hnRNPA1-Cry2 or DDX4-Cry2 fusion proteins do not phase separate in cells, unless the Cry2 protein is first triggered to assemble through specific light-activated interactions (see Figures 2B and 2C of Shin et al. [2016]). This observation highlights how specific oligomerization domains can act cooperatively with IDRs to promote LLPS in cells, and how some IDRs may be insufficient to undergo LLPS without additional oligomerization elements. As an example of the importance of non-specific interactions in promoting cellular LLPS, the C-terminal IDR of yeast Lsm4 can enhance yeast P-body formation, but it can be functionally replaced in this role by other IDRs (Decker et al., 2007). Moreover, polyQ rich tracts, which are disordered IDRs capable of diverse interactions, are prevalent in P-body components and RNA-binding proteins (Decker et al., 2007; Reijns et al., 2008), and can function in RNP granule assembly in *A. gossypii* (Lee et al., 2015). Similarly, the IDR of MEG-3 is not sufficient to from RNP granules in *C. elegans* embryos, unless the concentration of RNA in embryos was increased by preventing RNA turnover (Smith et al., 2016). Taken together, we suggest that many IDRs on RNA-binding proteins provide an additional layer of nonspecific interactions, and those interactions can contribute to granule formation when they synergize with more specific interactions to stabilize the macroscopic structure.

An important point is that, even when insufficient in themselves to promote LLPS, promiscuous IDRs can decrease the critical concentration for phase separation driven by more specific interactions. We demonstrate this phenomenon for phase separation of PTB and RNA *in vitro* (Figure 4) and for P-body assembly *in vivo* (Figure 6). This highlights that in a phase diagram describing an assembly based on specific and promiscuous interactions, the addition of promiscuous interactions can shift the system from an unassembled state to an assembled state (Figures 7A and 7B).

Not all IDRs will influence RNP granule formation in the same molecular manner. Some IDRs will provide specific interactions through SLiMs (Jonas and Izaurralde, 2013). Some IDRs may also afford interaction specificity through formation of local structure, such as LARKS (Hughes et al., 2017) or amyloid-like cross-beta interactions, that could be important in biological contexts where RNP granules need to be long-lived or mechanically stable (Boke and Mitchison, 2017; Kato et al., 2012) and that should show some sequence specificity. Charge patterning can also afford sequence specificity, although likely to a lower degree (Nott et al., 2015; Pak et al., 2016). Finally, as suggested here, some IDRs will provide promiscuous interactions that can enhance RNP granule assembly. Therefore, interactions undergone by any individual IDR that can contribute to intracellular LLPS likely lay on a scale from low affinity and highly promiscuous, to moderate affinity and selective.

A priori, there are three general classes of promiscuous interactions that IDRs could contribute to granule assembly. First, IDRs could interact with themselves or with other IDRs through weak interactions, which is suggested by observations that

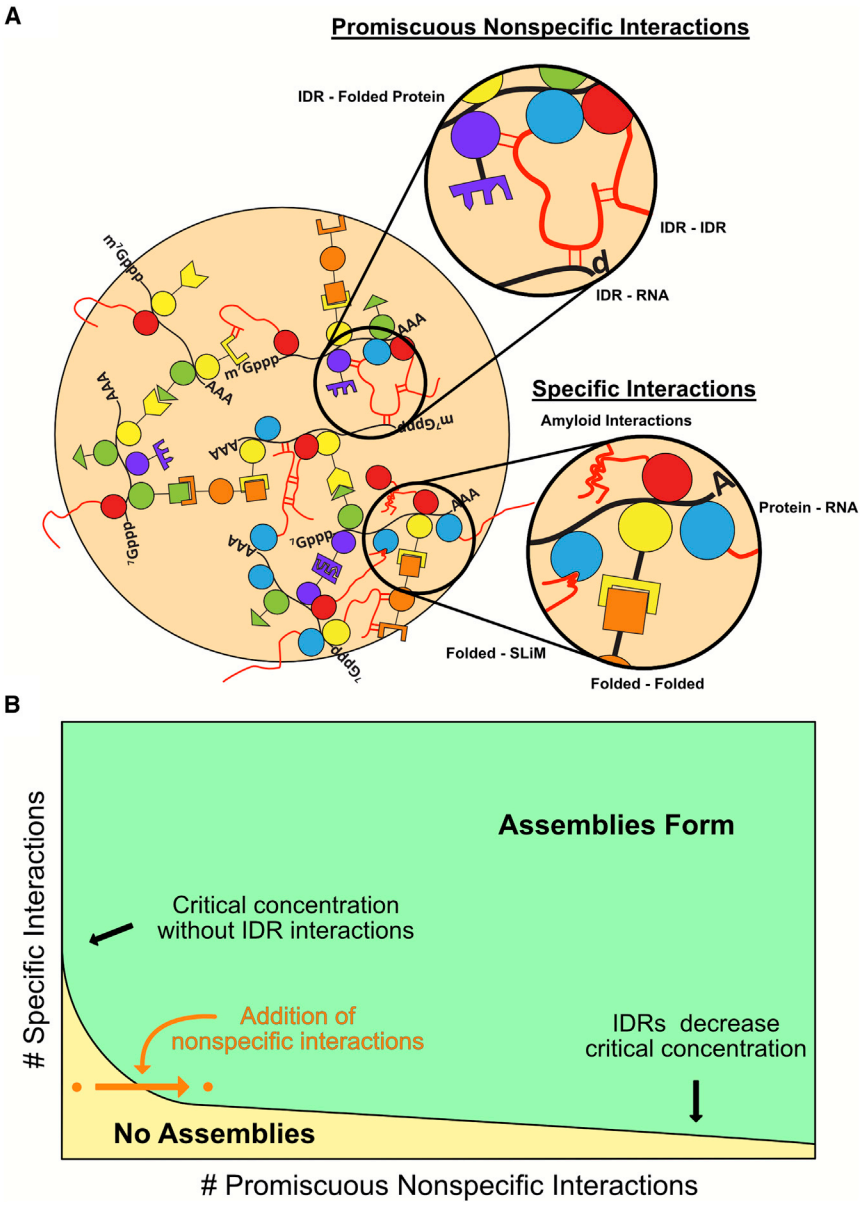

Figure 7. Model of RNP Granule Assembly and Contributions of IDRs

(A) RNP granules assembly by a wide variety of specific and nonspecific interactions.

(B) A theoretical phase diagram depicting how the addition of nonspecific, IDR-driven interactions could decrease the critical concentration of assembly for higher-order structures.

both IDR-based hydrogels and phase-separated liquid droplets can recruit proteins with different IDRs (Kato et al., 2012; Lin et al., 2015). Second, IDRs could have promiscuous interactions with RNAs, which is suggested by observations that some IDRs cross-link to RNA *in vivo* (Castello et al., 2016) and some IDRs bind RNA *in vitro* (Lin et al., 2015; Molliex et al., 2015). Finally, IDRs could make promiscuous interactions with other well-folded domains of granule components. Note that promiscuous interactions of IDRs with well-folded domains of proteins could provide an evolutionary starting point for the formation of SLiMs, which are often found in IDRs. An important future goal will be in determining how IDRs utilize each of these interaction types to contribution to granule formation.

Utilizing promiscuous nonspecific interactions of IDRs to modulate the assembly of macro-scale complexes has unique advantages. First, because such nonspecific interactions are not limited to defined components or stereospecific arrangements, they can interact promiscuously with any number of individual components to enhance assembly. For example, in RNP granules, a diversity of mRNPs with different RNA-binding proteins can be components of the granule. Promiscuous IDRs on RNA-binding proteins could interact with any of these mRNPs to enhance granule assembly. Moreover, IDRs can be subject to rapid evolution and control by post-translational modifications, thus making them ideal components to change granule assembly parameters under selective pressure and in response to signaling pathways. Finally, we note that because higher-order assemblies are large with respect to a single IDR, promiscuous interactions of IDRs will mostly occur within the quinary space of the assembly, rather than with proteins outside of the assembly. This makes large assemblies particularly well suited to enhancement by IDRs.

Macromolecular assembly and concomitant LLPS mediated by combinations of specific and promiscuous interactions is a general mechanism for forming dynamic, meso-scale structures in eukaryotic cells. Eukaryotic cells contain many such assemblies including RNP granules, signaling complexes, DNA damage repair foci, and transcription complexes. It is notable that components of all of these assemblies are enriched in IDRs (Banani et al., 2016; Hegde et al., 2010; Iakoucheva et al., 2002; Kai, 2016; Minezaki et al., 2006). Thus, we suggest that higher order complexes will often be assembled by a combination of specific interactions that drive assembly, reinforced by a network of promiscuous nonspecific IDR-based interactions, which stabilize the complex because of their physical coupling to specific assembly components. Such assemblies will be easily modified over time via evolution, or in a dynamic sense by signaling pathways and post-translational modification. This would occur without having to change the underlying specific assembly interactions, thus allowing both rapid evolution of and immediate control over intracellular assemblies.

EXPERIMENTAL PROCEDURES

Protein Purification and Labeling

Proteins were expressed and purified as previously reported (Lin et al., 2015). See also the Supplemental Experimental Procedures.

Droplet Assembly

Droplets were assembled as previously described (Lin et al., 2015). See also the Supplemental Experimental Procedures. Purified proteins were cleaved prior to droplet formation. Protease and purification tags were not removed. Where stated, FITC-conjugated lysozyme (Nanocs) and FITC-BSA (Thermo Fisher Scientific) were mixed with fusion proteins prior to assembly at 100 nM and 10 nM, respectively. BSA impairment at 100 mg/mL was repeated >3 times. Unless otherwise stated, assemblies were allowed to settle to the coverslip for between 1 and 2 hr.

Fluorescence Microscopy

All yeast experiments and images of SNAP-IDR and SNAP-hnRNPA1 were acquired on a DeltaVision epi-fluorescence microscope, with an SCMOS camera. All images of SNAP-PTB-IDR were acquired on a Leica-based spinning disk confocal microscope (EMCCD, ImagEM X2, Hamamatsu; confocal scanner unit, CSU-X1, Yokogawa).

Growth and Microscopy of P-Body Component Variants

To test the effect of Dhh1-IDR chimera on P-body recovery in the edc3Δ lsm4ΔC yeast (Strain yRP2338), yeast were transformed with vector only or vectors containing GFP fusions of Dhh1 wild-type, Dhh1-1-427, and Dhh1-IDR chimera using standard yeast transformation protocols. For P-body colocalization, strains with either Dcp2-GFP or Edc3-mCherry (tagged genomically) were transformed with IDR variants (Table S2). Biological replicates were grown overnight to saturation at 30°C with shaking in SD-Ura media (minimal media), containing 2% dextrose. Saturated cultures were re-inoculated into fresh SD-Ura media and grown to optical density (OD) = 0.4–0.5. Cells were pelleted and transferred to S-Ura media lacking dextrose and shaken at 30°C for 10 min (P-body rescue) or 15 min (P-body colocalization) prior to imaging. When unstressed the cells were pelleted without glucose starvation.

Images were quantified manually using FIJI. For P-body colocalization accuracy, single slices were used and analysis was blinded. P-bodies were identified by either Dcp2-GFP or Edc3-mCherry and then variant localization assessed. Manual assessment is required due to the common variability of expression between cells.

Statistical Methods

For droplet size, the Welch's t test for unequal variance was used, SciPy Statistics Module, n = 3 images. For Dhh1 rescue experiments $\geq$2 images from 3 biological replicates were counted, and the Student's t test in Microsoft Excel used.

SUPPLEMENTAL INFORMATION

Supplemental Information includes Supplemental Experimental Procedures, three figures, and two tables and can be found with this article online at https://doi.org/10.1016/j.celrep.2018.01.036.

ACKNOWLEDGMENTS

This work was initiated and supported by an HCIA grant from the Howard Hughes Medical Institute, and we thank all members of the HHMI/MBL Summer Institute for their intellectual contributions. D.S.W.P. was supported by T32 GM063235. Work in R.P.'s laboratory was supported by NIH (GM045443) and the Howard Hughes Medical Institute. Work in M.K.R.'s lab was supported by the Howard Hughes Medical Institute and grants from the NIH (R01-GM56322) and Welch Foundation (I-1544).

AUTHOR CONTRIBUTIONS

D.S.W.P. designed and performed experiments, provided substantial intellectual input, contributed to writing the paper, and edited the paper. B.V.T. and B.S.R. designed and performed experiments and edited the paper. Y.L. designed and performed experiments, provided substantial intellectual input, and edited the paper. L.M. performed experiments. M.K.R. provided substantial intellectual input, assisted with experimental design, and edited the paper. R.P. provided substantial intellectual input, assisted with experimental design, contributed to writing the paper, and edited the paper.

DECLARATION OF INTERESTS

The authors declare no competing interests.

Received: February 14, 2017
Revised: November 30, 2017
Accepted: January 11, 2018
Published: February 6, 2018

REFERENCES

Banani, S.F., Rice, A.M., Peeples, W.B., Lin, Y., Jain, S., Parker, R., and Rosen, M.K. (2016). Compositional control of phase-separated cellular bodies. Cell *166*, 651–663.

Boke, E., and Mitchison, T.J. (2017). The balbiani body and the concept of physiological amyloids. Cell Cycle *16*, 153–154.

Brangwynne, C.P. (2013). Phase transitions and size scaling of membrane-less organelles. J. Cell Biol. *203*, 875–881.

Brangwynne, C.P., Eckmann, C.R., Courson, D.S., Rybarska, A., Hoege, C., Gharakhani, J., Jülicher, F., and Hyman, A.A. (2009). Germline P granules are liquid droplets that localize by controlled dissolution/condensation. Science *324*, 1729–1732.

Brangwynne, C.P., Tompa, P., and Pappu, R.V. (2015). Polymer physics of intracellular phase transitions. Nat. Phys. *11*, 899–904.

Castello, A., Fischer, B., Frese, C.K., Horos, R., Alleaume, A.-M., Foehr, S., Curk, T., Krijgsveld, J., and Hentze, M.W. (2016). Comprehensive identification of RNA-binding domains in human cells. Mol. Cell *63*, 696–710.

Conicella, A.E., Zerze, G.H., Mittal, J., and Fawzi, N.L. (2016). ALS mutations disrupt phase separation mediated by α-helical structure in the TDP-43 low-complexity C-terminal domain. Structure *24*, 1537–1549.

Das, R.K., Ruff, K.M., and Pappu, R.V. (2015). Relating sequence encoded information to form and function of intrinsically disordered proteins. Curr. Opin. Struct. Biol. *32*, 102–112.

Decker, C.J., Teixeira, D., and Parker, R. (2007). Edc3p and a glutamine/asparagine-rich domain of Lsm4p function in processing body assembly in Saccharomyces cerevisiae. J. Cell Biol. *179*, 437–449.

Elbaum-Garfinkle, S., Kim, Y., Szczepaniak, K., Chen, C.C.-H., Eckmann, C.R., Myong, S., and Brangwynne, C.P. (2015). The disordered P granule protein LAF-1 drives phase separation into droplets with tunable viscosity and dynamics. Proc. Natl. Acad. Sci. USA *112*, 7189–7194.

Feric, M., Vaidya, N., Harmon, T.S., Mitrea, D.M., Zhu, L., Richardson, T.M., Kriwacki, R.W., Pappu, R.V., and Brangwynne, C.P. (2016). Coexisting liquid phases underlie nucleolar subcompartments. Cell *165*, 1686–1697.

Fromm, S.A., Kamenz, J., Nöldeke, E.R., Neu, A., Zocher, G., and Sprangers, R. (2014). In vitro reconstitution of a cellular phase-transition process that involves the mRNA decapping machinery. Angew. Chem. Int. Ed. Engl. *53*, 7354–7359.

Gilks, N., Kedersha, N., Ayodele, M., Shen, L., Stoecklin, G., Dember, L.M., and Anderson, P. (2004). Stress granule assembly is mediated by prion-like aggregation of TIA-1. Mol. Biol. Cell *15*, 5383–5398.

Hand, S.C., Menze, M.A., Toner, M., Boswell, L., and Moore, D. (2011). LEA proteins during water stress: not just for plants anymore. Annu. Rev. Physiol. *73*, 115–134.

Harigaya, Y., Jones, B.N., Muhlrad, D., Gross, J.D., and Parker, R. (2010). Identification and analysis of the interaction between Edc3 and Dcp2 in Saccharomyces cerevisiae. Mol. Cell. Biol. *30*, 1446–1456.

Hegde, M.L., Hazra, T.K., and Mitra, S. (2010). Functions of disordered regions in mammalian early base excision repair proteins. Cell. Mol. Life Sci. *67*, 3573–3587.

Hennig, S., Kong, G., Mannen, T., Sadowska, A., Kobelke, S., Blythe, A., Knott, G.J., Iyer, K.S., Ho, D., Newcombe, E.A., et al. (2015). Prion-like domains in RNA binding proteins are essential for building subnuclear paraspeckles. J. Cell Biol. *210*, 529–539.

Hughes, M.P., Sawaya, M.R., Goldschmidt, L., Rodriguez, J.A., Cascio, D., Gonen, T., and Eisenberg, D.S. (2017). Low-complexity domains adhere by reversible amyloid-like interactions between kinked β-sheets. bioRxiv. https://doi.org/10.1101/153817.

Iakoucheva, L.M., Brown, C.J., Lawson, J.D., Obradović, Z., and Dunker, A.K. (2002). Intrinsic disorder in cell-signaling and cancer-associated proteins. J. Mol. Biol. *323*, 573–584.

Jain, S., Wheeler, J.R., Walters, R.W., Agrawal, A., Barsic, A., and Parker, R. (2016). ATPase-modulated stress granules contain a diverse proteome and substructure. Cell *164*, 487–498.

Jencks, W.P. (1981). On the attribution and additivity of binding energies. Proc. Natl. Acad. Sci. USA *78*, 4046–4050.

Jonas, S., and Izaurralde, E. (2013). The role of disordered protein regions in the assembly of decapping complexes and RNP granules. Genes Dev. *27*, 2628–2641.

Kai, M. (2016). Roles of RNA-binding proteins in DNA damage response. Int. J. Mol. Sci. *17*, 310.

Kato, M., Han, T.W., Xie, S., Shi, K., Du, X., Wu, L.C., Mirzaei, H., Goldsmith, E.J., Longgood, J., Pei, J., et al. (2012). Cell-free formation of RNA granules: low complexity sequence domains form dynamic fibers within hydrogels. Cell *149*, 753–767.

Kedersha, N., Panas, M.D., Achorn, C.A., Lyons, S., Tisdale, S., Hickman, T., Thomas, M., Lieberman, J., McInerney, G.M., Ivanov, P., and Anderson, P. (2016). G3BP-Caprin1-USP10 complexes mediate stress granule condensation and associate with 40S subunits. J. Cell Biol. *212*, 845–860.

Kim, H.J., Kim, N.C., Wang, Y.-D., Scarborough, E.A., Moore, J., Diaz, Z., MacLea, K.S., Freibaum, B., Li, S., Molliex, A., et al. (2013). Mutations in prion-like domains in hnRNPA2B1 and hnRNPA1 cause multisystem proteinopathy and ALS. Nature *495*, 467–473.

Lee, C., Occhipinti, P., and Gladfelter, A.S. (2015). PolyQ-dependent RNA-protein assemblies control symmetry breaking. J. Cell Biol. *208*, 533–544.

Li, P., Banjade, S., Cheng, H.-C., Kim, S., Chen, B., Guo, L., Llaguno, M., Hollingsworth, J.V., King, D.S., Banani, S.F., et al. (2012). Phase transitions in the assembly of multivalent signalling proteins. Nature *483*, 336–340.

Lin, Y., Protter, D.S.W., Rosen, M.K., and Parker, R. (2015). Formation and maturation of phase-separated liquid droplets by RNA-binding proteins. Mol. Cell *60*, 208–219.

Lin, Y.-H., Forman-Kay, J.D., and Chan, H.S. (2016). Sequence-specific polyampholyte phase separation in membraneless organelles. Phys. Rev. Lett. *117*, 178101.

Milo, R. (2013). What is the total number of protein molecules per cell volume? A call to rethink some published values. BioEssays *35*, 1050–1055.

Minezaki, Y., Homma, K., Kinjo, A.R., and Nishikawa, K. (2006). Human transcription factors contain a high fraction of intrinsically disordered regions essential for transcriptional regulation. J. Mol. Biol. *359*, 1137–1149.

Mitrea, D.M., Cika, J.A., Guy, C.S., Ban, D., Banerjee, P.R., Stanley, C.B., Nourse, A., Deniz, A.A., and Kriwacki, R.W. (2016). Nucleophosmin integrates within the nucleolus via multi-modal interactions with proteins displaying R-rich linear motifs and rRNA. eLife *5*, e13571.

Molliex, A., Temirov, J., Lee, J., Coughlin, M., Kanagaraj, A.P., Kim, H.J., Mittag, T., and Taylor, J.P. (2015). Phase separation by low complexity domains promotes stress granule assembly and drives pathological fibrillization. Cell *163*, 123–133.

Nott, T.J., Petsalaki, E., Farber, P., Jervis, D., Fussner, E., Plochowietz, A., Craggs, T.D., Bazett-Jones, D.P., Pawson, T., Forman-Kay, J.D., and Baldwin, A.J. (2015). Phase transition of a disordered nuage protein generates environmentally responsive membraneless organelles. Mol. Cell *57*, 936–947.

Pak, C.W., Kosno, M., Holehouse, A.S., Padrick, S.B., Mittal, A., Ali, R., Yunus, A.A., Liu, D.R., Pappu, R.V., and Rosen, M.K. (2016). Sequence Determinants of Intracellular Phase Separation by Complex Coacervation of a Disordered Protein. Mol. Cell *63*, 72–85.

Patel, A., Lee, H.O., Jawerth, L., Maharana, S., Jahnel, M., Hein, M.Y., Stoynov, S., Mahamid, J., Saha, S., Franzmann, T.M., et al. (2015). A liquid-to-solid phase transition of the ALS protein FUS accelerated by disease mutation. Cell *162*, 1066–1077.

Rao, B.S., and Parker, R. (2017). Numerous interactions act redundantly to assemble a tunable size of P bodies in *Saccharomyces cerevisiae*. Proc. Natl. Acad. Sci. USA *114*, E9569–E9578.

Reijns, M.A.M., Alexander, R.D., Spiller, M.P., and Beggs, J.D. (2008). A role for Q/N-rich aggregation-prone regions in P-body localization. J. Cell Sci. *121*, 2463–2472.

Shin, Y., Berry, J., Pannucci, N., Haataja, M.P., Toettcher, J.E., and Brangwynne, C.P. (2016). Spatiotemporal control of intracellular phase transitions using light-activated optoDroplets. Cell *168*, 159–171.

Smith, J., Calidas, D., Schmidt, H., Lu, T., Rasoloson, D., and Seydoux, G. (2016). Spatioal patterning of P granules by RNA-induced phase separation of the intrinsically-disordered protein MEG-3. eLife. https://doi.org/10.7554/eLife.21337.

Spector, D.L. (2006). SnapShot: cellular bodies. Cell *127*, 1071.

Xiang, S., Kato, M., Wu, L.C., Lin, Y., Ding, M., Zhang, Y., Yu, Y., and McKnight, S.L. (2015). The LC domain of hnRNPA2 adopts similar conformations in hydrogel polymers, liquid-like droplets, and nuclei. Cell *163*, 829–839.

Zhang, H., Elbaum-Garfinkle, S., Langdon, E.M., Taylor, N., Occhipinti, P., Bridges, A.A., Brangwynne, C.P., and Gladfelter, A.S. (2015). RNA controls PolyQ protein phase transitions. Mol. Cell *60*, 220–230.

Cell Reports, Volume *22*

Supplemental Information

Intrinsically Disordered Regions Can Contribute Promiscuous Interactions to RNP Granule Assembly

David S.W. Protter, Bhalchandra S. Rao, Briana Van Treeck, Yuan Lin, Laura Mizoue, Michael K. Rosen, and Roy Parker

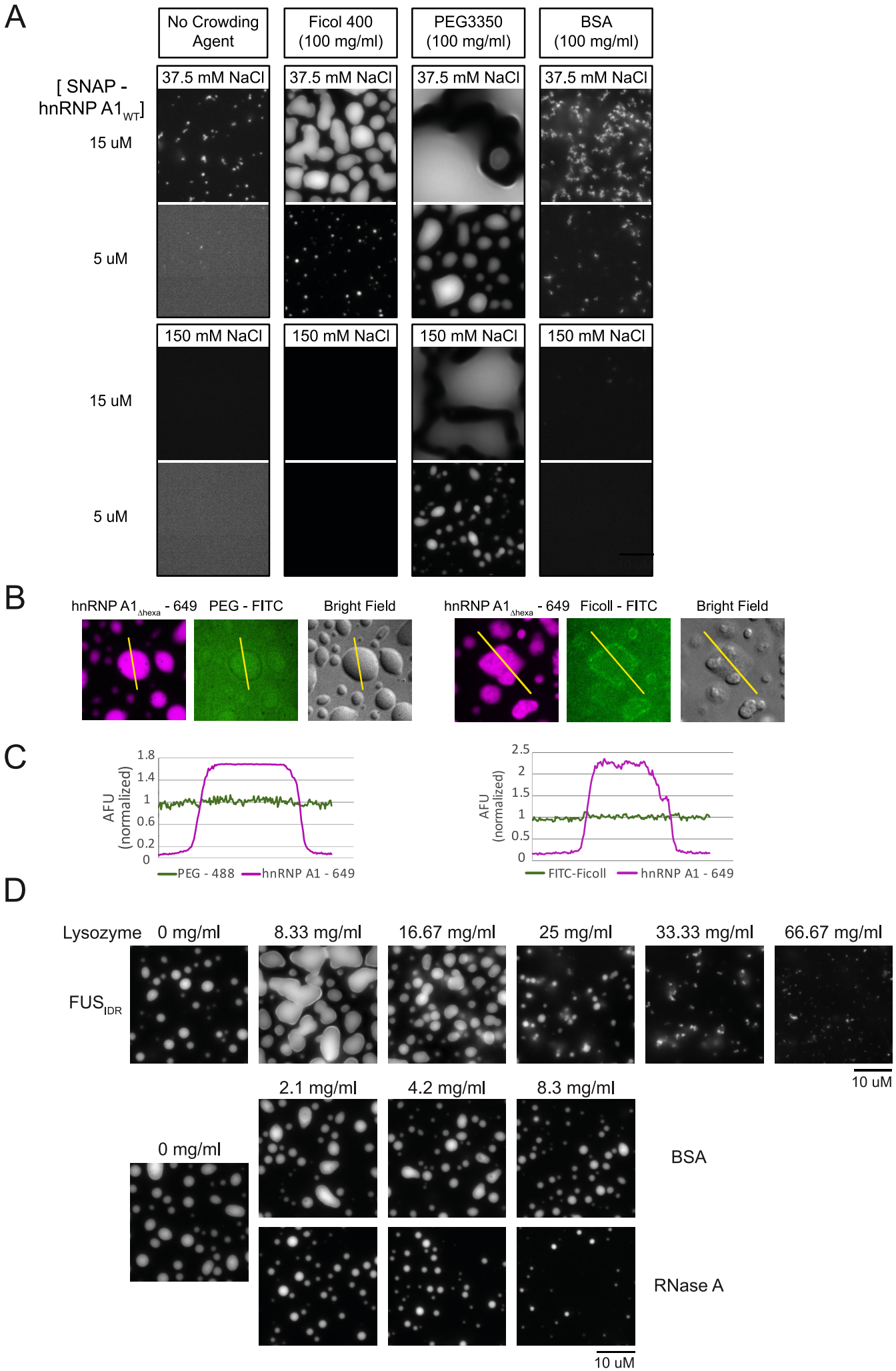
A
No Crowding Agent
Ficol 400 (100 mg/ml)
PEG3350 (100 mg/ml)
BSA (100 mg/ml)
[SNAP - hnRNP A1WT]
37.5 mM NaCl
150 mM NaCl
15 uM
5 uM
B
hnRNP A1Δhexa - 649
PEG - FITC
Bright Field
Ficoll - FITC
C
AFU (normalized)
PEG - 488
hnRNP A1 - 649
FITC-Ficoll
D
Lysozyme
0 mg/ml
8.33 mg/ml
16.67 mg/ml
25 mg/ml
33.33 mg/ml
66.67 mg/ml
FUSIDR
10 uM
2.1 mg/ml
4.2 mg/ml
8.3 mg/ml
BSA
RNase A

Figure S1: Diverse Effects of Crowding Agents on LLPS, related to Figures 1 and 2

(A) Fluorescence microscope images of structures formed by SNAP-hnRNP A1 at either 150 mM NaCl or 37.5 mM NaCl in the absence or presence of 100 mg/ml Ficoll 400, PEG 3350, or BSA. SNAP-hnRNP A1 concentrations were either 15μM or 5μM and assemblies were allowed to settle for 7.5 hrs.

(B) Fluorescent images of droplets of SNAP-hnRNP $A1_{\Delta hexa}$ in the presence of FITC-PEG or FITC-Ficoll. Conditions were 10% PEG, 150 mM NaCl, 25μM SNAP-hnRNP $A1_{\Delta hexa}$ and 10% Ficoll, 100 mM NaCl, 50μMSNAP-hnRNP $A1_{\Delta hexa}$. Both reactions had 20mM Tris, pH 7.4.

(C) Line traces across droplets showing no enrichment of FITC-PEG or FITC-Ficoll.

(D) Fluorescence microscope images of structures formed by SNAP-FUS_{IDR} while being titrated with either Lysozyme, BSA, or RNAse A

Variant	Amino Acids
Dhh1ΔIDR	1-427
Dhh1 IDR	427-506
Ccr4ΔIDR	148-837
Ccr4 IDR	1-229
Pop2ΔIDR	147-433
Pop2 IDR	1-156
Lsm4ΔIDR	1-90,
Lsm4 IDR	91-187

Table S1: Yeast RNA Binding Protein Variants related to Figure 5
Protein variants and the amino acids included from the original protein.

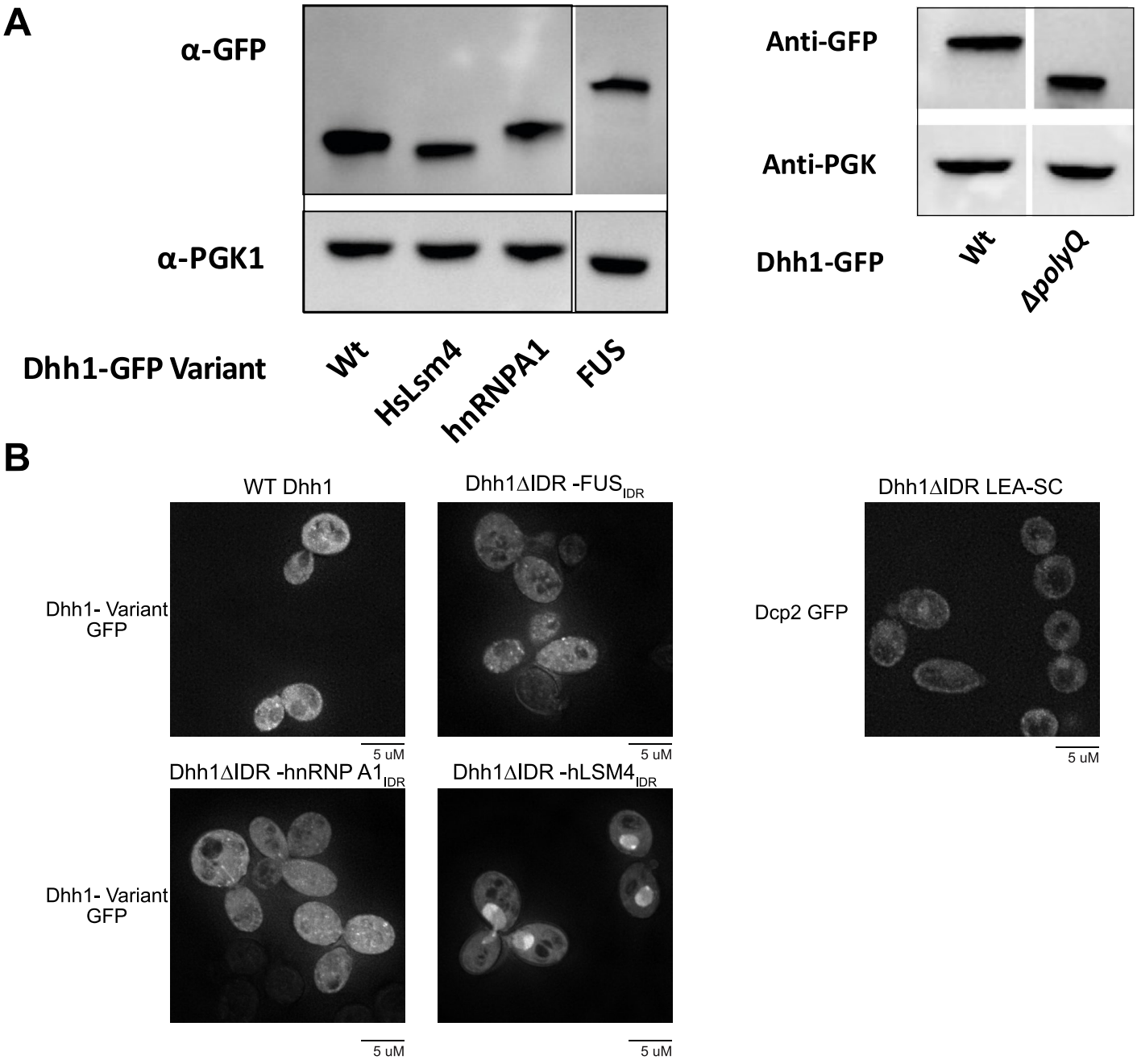

Figure S2: Dhh1 IDR Fusions Do Not Form Large Assemblies in the Absence of Stress, related to Figure 6

(A) Western blot of Dhh1 variant expression

(B) Fluorescent microscopy images of cells expressing Dhh1-GFP, either genomically or as a plasmid-expressed Dhh1-GFP variant. Cells were growing under log phase growth conditions just prior to imaging. Large regions of fluorescence in Dhh1ΔIDR-hLsm4$_{IDR}$ show nuclear localization of the construct. LEA-SC Dhh1 variant is visualized by Dcp2GFP.

A

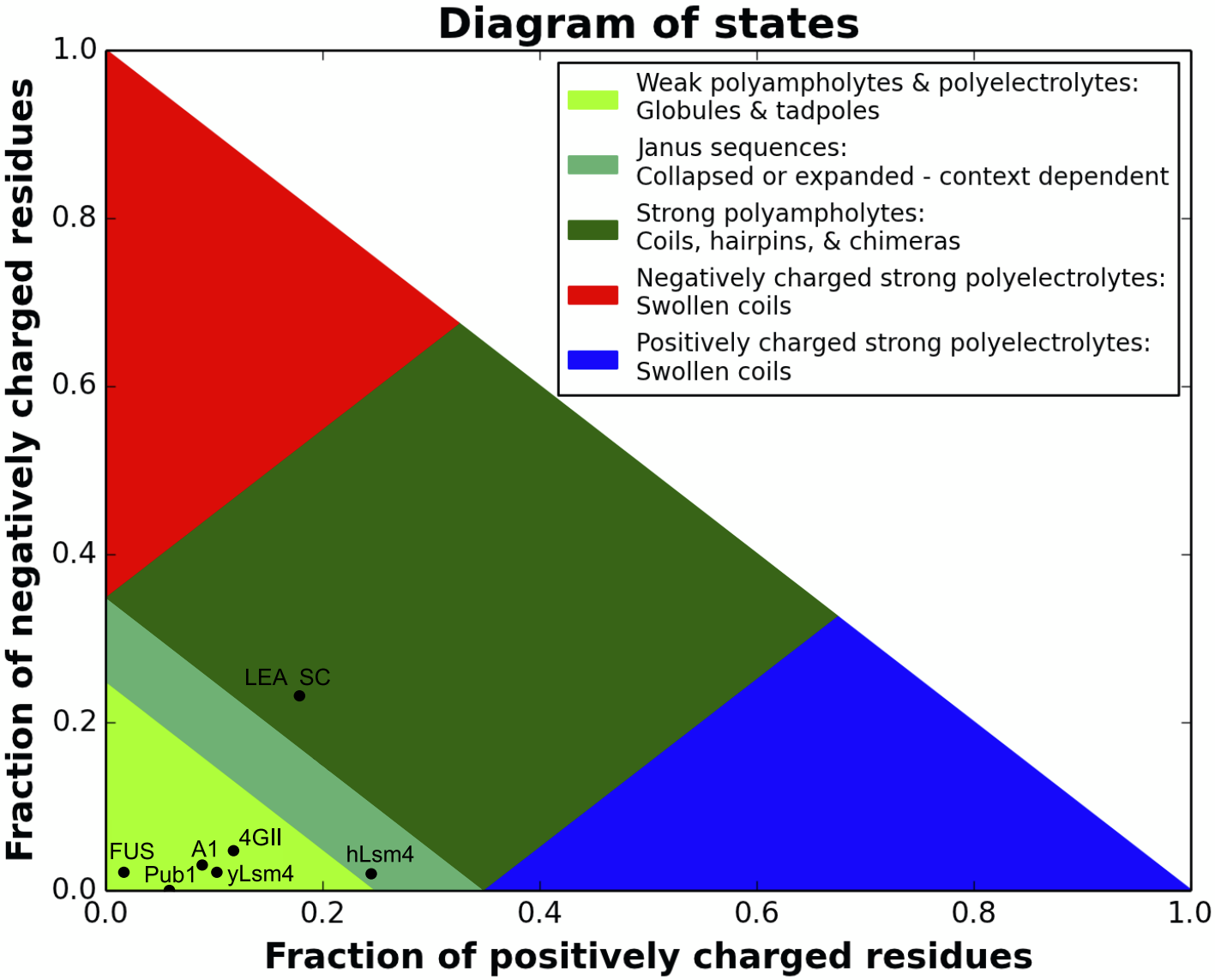

B

IDR	N	f-	f+	FCR	NCPR	Kappa
hnRNP A1	135	0.02963	0.08889	0.11852	0.05926	0.21457
FUS	237	0.0211	0.01688	0.03797	-0.00422	0.28624
4GII	85	0.04706	0.11765	0.16471	0.07059	0.21608
yLsm4	97	0.02062	0.10309	0.12371	0.08247	0.2373
hLsm4	53	0.01887	0.24528	0.26415	0.22642	0.11459
Pub1	85	0	0.05882	0.05882	0.05882	0.34311
LEA SC	95	0.23158	0.17895	0.41053	-0.05263	0.02806

Figure S3: Analysis of IDR Composition and Predicted Solution Behavior, related to Figures 1, 2, 3, 4, 5, and 6

(A) Diagram of IDR solution state predicted by CIDER (Das et al., 2015).

(B) Table of physical parameters from CIDER. N = Number of amino acids. f- and f+ = fraction negatively and positively charged residues, respectively. FCR = Fraction Charged Residues. NCPR = Net Charge Per Residue. Kappa = a measure of homogenous charge distribution, with values between 0 and 1 where lower values represent a more homogeneous charge distribution.

Supplemental Methods

Protein Purification

Proteins were expressed from the pMal-c2 vector (NEB), except for full length hnRNPA1 and related mutants, which were cloned into a modified pet11a vector (Novagen). Proteins were expressed in *E. coli* BL21(DE3) and purified with Ni-NTA and/or amylose resin under standard conditions. SNAP-PTB-IDRs were further purified through a Superdex200 column (GE Healthcare). Proteins were fluorescently-labeled with SNAP-Surface 488 or SNAP-Surface 649 (NEB) according to the manufacturer's protocols. Unincorporated dye was removed using Zeba Spin Desalting Columns, 7K MWCO (Thermo Fisher). Proteins were concentrated using Amicon Ultra 10K MWCO centrifugal filters (Milipore) and aggregates removed by ultra-centrifugation at 4°C for 30' at 50K RPM in a Beckman-Coulter TLA 100.2 rotor.

Droplet Quantification:

Images were analyzed in FIJI. Maximal Z-projections were made when necessary (hnRNP A1Δhexa droplets), and then thresholded using either 'Default' (hnRNP A1 Δhexa droplets) or "Otsu" (PTB droplets) ('Threshold'). Binary images were eroded ('Erode') once to remove single pixels, then dialated ('Dialate') once to return droplets to their original size. This was followed by watershedding ('Watershed') to separate proximal droplets. FIJIs 'Analyze Particles' was used to generate ROIs, which were used to measure the maximal intensity projection, generating area and mean intensity values for each assembly. Three independent fields of view from each condition were used.

Droplet Assembly

For SNAP-IDRs SNAP-hnRNPA1 (~2% fluorescently labeled), droplet assembly was initiated by diluting solutions to 37.5 mM NaCl, 20 mM Tris pH 7.4, 1 mM DTT. For SNAP-PTB-IDRs, proteins and RNA, $(UCUCUAAAAA)_5$, were mixed at the indicated concentrations (including 100 nM SNAP-PTB-IDRs labeled with SNAP-Surface 649) in 100 mM NaCl, 20 mM imidazole pH 7.0, 1 mM DTT, 10% glycerol. N-terminal purification tags of SNAP-hnRNPA1 were removed by HRV C3 protease (EMD Milipore) during the dye conjugation step (Lin et al., 2015). Neither the protease nor the 6XHIS-MBP purification tags were removed prior to droplet assembly. N-terminal MBP and C-terminal His tags of SNAP-IDRs and SNAP-PTB-IDRs were cleaved just prior to droplet assembly with TEV protease (Promega ProTEV). Neither the protease nor the MBP and 6XHis purification tags were removed prior to droplet assembly. Reactions were performed in glass-bottom chambers passivated with 3% BSA.

Yeast Lysate Preparation:

Yeast lysates were prepared from BY4741 frozen cell pellets from 50mL cultures grown in rich media, at log phase. Pellets were resuspended in small volumes of lysis buffer (50 mM Tris-HCl, pH 7.4, 100 mM KoAc, 2 mM $Mg(oAc)_2$ 50 μg/mL Heparin, 0.5 mM DTT, 0.5% NP40, EDTA free protease inhibitor). Approximately 500 μL of acid-washed glass beads (Sigma G8772) were added for bead lysis. Cells were lysed by vortexing on high speed for 2 min followed by 2 min sitting on ice, repeated three times. A heated 18-gauge needle was used to puncture the bottom of the microfuge tube. The microfuge tube was placed in a 10mL conical, and the lysate was collected by centrifugation for 2 min at 805 rcf. The semi-clarified extract was further spun at 21000 rcf for 10min in the cold room. The clarified extract was collected and the buffer was exchanged with

droplet assembly buffer (37.5 mM NaCl, 20 mM Tris pH 7.4, 1 mM DTT) by sequential use of two 7K MWCO Zeba desalting columns. This likely also removed most small molecules, nucleotides, etc from the lysate. The lysate was then spun for 15 minutes in a TLA 100.2 ultracentrifuge rotor at 50,000 rpm for 30 min. Approximate lysate concentration was quantified using a NanoDrop spectrophotometer.

Plasmid construction

The Dhh1-GFP gene fragment containing the Dhh1 promoter was PCR amplified using the genomic DNA from the Dhh1-GFP yeast strain (yeast GFP collection) and BSR_DhhGFP416NF and BSR_DhhGFP416NR primers. The Adh1 terminator fragment was clone using the primers BSR_Adh1SacF and BSR_Adh1SacR. The Dhh1-GFP and Adh1 terminator fragments were inserted sequentially into the XhoI and SacI digested pRS416 vector, respectively, via Infusion cloning (Takara). The poly P/Q residues of Dhh1 (428-506 were deleted from the Dhh1-GFP containing vector using primers, Dhh11-427F and Dhh11-427R via the Phusion mutagenesis protocol (Thermo Fisher). Lastly, the intron-less IDR sequence for HsLsm4 was synthesized using gBLOCK technology from IDT technologies. The IDRs were PCR amplified using primers, BSR_427FUSF and BSR_427FUSR, BSR_427A1F and BSR_427A1R, BSR_427HsLsm4F and BSR_427HsLsm4R, for FUS, hnRNPA1 and HsLsm4, respectively and cloned into the linearized Dhh1-1-427-GFP vector using Infusion cloning.